Loading-induced anti-tumor capability of murine and human urine

Di Wu[1,2], Yao Fan[1, 2], Shengzhi Liu[2], Mark D. Woollam[3,4], Xun Sun[1,2], Eiji Murao[2, 5], Rongrong Zha[1, 2], Rahul Prakash[2], Charles Park[6], Amanda P. Siegel[3, 4], Jing Liu[6, 7], Mangilal Agarwal[4], Bai-Yan Li[1*], and Hiroki Yokota[1, 2, 4, 7, 8*]

[1]Department of Pharmacology, School of Pharmacy, Harbin Medical University, Harbin 150081, China
[2]Department of Biomedical Engineering, Indiana University Purdue University Indianapolis, Indianapolis, IN 46202, USA
[3]Department of Chemistry and Chemical Biology, Indiana University Purdue University Indianapolis, Indianapolis, IN 46202, USA
[4]Integrative Nanosystems Development Institute, Indiana University Purdue University Indianapolis, Indianapolis, IN 46202, USA
[5]Graduate School of Engineering, Mie University, Mie 514, Japan
[6]Department of Physics, Indiana University Purdue University Indianapolis, Indianapolis, IN 46202, USA
[7]Simon Cancer Research Center, Indiana University School of Medicine, Indianapolis, IN 46202, USA
[8]Indiana Center for Musculoskeletal Health, Indiana University School of Medicine, Indianapolis, IN 46202, USA

Keywords: urine, loading, breast cancer, tumor progression, cholesterol, dopamine, melatonin, Lrp5, CSF1, CD105, TCGA
Running title: Loading and Urine's Anti-Tumor Capability

*Co-Corresponding Authors:

Hiroki Yokota, PhD
Department of Biomedical Engineering
Indiana U. Purdue U. Indianapolis
723 West Michigan Street, SL220
Indianapolis, IN 46202 USA
Phone: 317-278-5177
Fax: 317-278-2455
Email: hyokota@iupui.edu

Bai-Yan Li, MD/PhD
Department of Pharmacology
School of Pharmacy, Harbin Medical University
#157 Baojian Road
Harbin 150081, China
Phone/Fax: +86 451-8667-134

E-mail: liby@ems.hrbmu.edu.cn

This is the author's manuscript of the article published in final edited form as:

Wu, D., Fan, Y., Liu, S., Woollam, M. D., Sun, X., Murao, E., Zha, R., Prakash, R., Park, C., Siegel, A. P., Liu, J., Agarwal, M., Li, B.-Y., & Yokota, H. (2020). Loading-induced antitumor capability of murine and human urine. FASEB Journal: Official Publication of the Federation of American Societies for Experimental Biology, 34(6), 7578–7592. https://doi.org/10.1096/fj.202000096R

Nonstandard Abbreviations

ANOVA: Analysis of variance; CD105: endoglin; CSF1: macrophage colony-stimulating factor 1; FRET: fluorescence resonance energy transfer; GTEx: Genotype-Tissue Expression; MMP9: matrix metalloproteinase 9; PPARγ: peroxisome proliferator-activated receptor gamma; TCGA: The Cancer Genome Atlas; TPM: transcript per million; UM: urine medium; VOCs: Volatile organic compounds.

Abstract

While urine has been considered as a useful bio-fluid for health monitoring, its dynamic changes to physical activity are not well understood. We examined urine's possible anti-tumor capability in response to medium-level, loading-driven physical activity. Urine was collected from mice subjected to 5-min skeletal loading and human individuals before and after 30-min step aerobics. Six cancer cell lines (breast, prostate, and pancreas) and a mouse model of the mammary tumor were employed to evaluate the effect of urine. Compared to urine collected prior to loading, urine collected post-activity decreased cellular viability, proliferation, migration, and invasion of tumor cells, as well as tumor weight in the mammary fat pad. Detection of urinary volatile organic compounds and ELISA assays showed that the loading-conditioned urine reduced cholesterol and elevated dopamine and melatonin. Immunohistochemical fluorescent images presented upregulation of the rate-limiting enzymes for the production of dopamine and melatonin in the brain. Molecular analysis revealed that the anti-tumor effect was linked to the reduction in molecular vinculin-linked molecular force as well as the downregulation of the Lrp5-CSF1-CD105 regulatory axis. Notably, the survival rate for the high expression levels of Lrp5, CSF1, and CD105 in tumor tissues was significantly lowered in the Cancer Genome Atlas database. Collectively, this study revealed that 5- or 10-min loading-driven physical activity was sufficient to induce the striking anti-tumor effect by activating neuronal signaling and repressing cholesterol synthesis. The result supported the dual role of loading-conditioned urine as a potential tumor suppressor and a source of diagnostic biomarkers.

Introduction

Ancient European and Asian texts prescribed therapeutic application of urine for a wide spectrum of life-threatening illnesses (1-3). In the early 20th century, a collection of anecdotal records, "The Water of Life: A treatise on urine therapy" came to be considered the founding document of the field (4, 5). Since cancer in many cases requires agents that induce life-threatening side effects, the possibility that a simple substance such as one's own urine could serve as a cancer treatment sparked interest (6-9). However, the existing body of scientific literature does not describe the therapeutic role of any specific components in urine.

While urine is a highly dynamic mixture (10), our particular focus is the effect of physical activity. Physical activity has been documented to induce multiple remedial effects and is recommended for innumerable health conditions (11-13). Several studies show that moderate exercise can selectively improve a cancer patient's prognosis by limiting tumor growth and preventing metastasis (14-16). Physical activity-conditioned serum from human patients was shown to decrease tumor cell viability and inhibit tumorigenesis in breast cancer cells (17-19). If physical activity induces anti-tumor properties in serum, a logical question is whether urine, a direct product of bloodstream filtration, may act as an anti-tumor agent. We also aimed to understand the role of physical activity in cancer progression.

Urine can be obtained noninvasively in significant amounts. Physical activity is known to alter lipid metabolism (20), and activate Wnt signaling in the skeleton and neuronal signaling in the brain (21-23). As specific urinary components, we first focused on cholesterol, dopamine, and melatonin, in which cholesterol is linked to lipid metabolism and dopamine and melatonin

neuronal signaling (24-28). We hypothesized that mechanical stimulation alters lipid metabolism and neuronal signaling, and induce anti-tumor effects in the urine. In searching for the potential mechanism of differentiating unconditioned urine medium (UM)from loading-conditioned UM, we examined the role of Lrp5 and Lrp6, co-receptors of Wnt signaling (29). We also evaluated the role of macrophage colony-stimulating factor 1 (CSF1), which is linked to bone homeostasis and the progression of many cancers (30).

Volatile organic compounds (VOCs) were also analyzed before and after physical activity. Focusing on the samples collected after skeletal loading, we examined whether VOCs could act as potential stimulators of synthesis of dopamine and melatonin. To evaluate the migratory capability of tumor cells, we evaluated tensile forces at focal adhesion sites of individual tumor cells using a FRET (fluorescence resonance energy transfer) -based vinculin tension sensor (31, 32). To evaluate the role of the key regulatory genes in cancer patients, we conducted bioinformatics analysis using TCGA (The Cancer Genome Atlas) and GTEx (Genotype-Tissue Expression) datasets.

Materials and Methods

Animal model and urine collection

8-week-old female C57BL/6 mice (Envigo, Indianapolis, IN, USA) were housed in standard rodent housing at a constant temperature, humidity, and a 12-hr light/dark cycle. The experimental procedures were approved by the Indiana University Animal Care and Use Committee. All experiments and methods were performed in accordance with relevant guidelines and regulations. Tibia loading was applied to 20 C57BL/6 female mice using an ElectroForce device (TA instruments, New Castle, DE, USA). Tibia loading has been frequently used as a load-bearing modality to study mechanotransduction of bone (33). Based on our previous study, loads were given to the left tibia with 5 N (peak-to-peak) at 2 Hz for 5 min (34). The control group was anesthetized and received sham loading without dynamic loads. Urine was collected before and 1 h or 2 h after tibia loading. In the mouse model of breast cancer, mice (12/group) received an injection of EO771 mammary tumor cells (3×10^5 cells in 20 μl PBS) to the mammary fat pad. Mice received diluted urine (20% dilution in 20 μl PBS) every other day as s.c. injection to the mammary fat pad, while mice in the control group received PBS.

Human urine collection

The use of human urine was approved by the Indiana University Institutional Review Board. Written informed consent was obtained from 10 healthy participants with no history of cancers (5 male and 5 female; average age, 28 ± 7 years in the range of 18 to 41), and urine samples were collected before and 1 h after 30-min step aerobics. The procedure included 10-min warming up at 80 beats per minute (bpm), 10-min core step aerobics at 120 bpm, and 10-min cooling down at 80 bpm.

Cell culture

EO771 mammary tumor cells (CH3 BioSystems, Amherst, NY, USA) (35), 4T1.2 mammary tumor cells (36), MDA-MB-231 breast cancer cells (ATCC, Manassas, VA, USA), MDA-MB-231-derived cell line, TMD cells (37), PC-3 human prostate cancer cells (ATCC) (38), PANC-1 human pancreatic cancer cells (ATCC) (39), and GnRH mouse hypothalamic neuronal cells (GT1-7; Sigma, Saint Louis, MO, USA) were grown in DMEM (Corning, Inc., Corning, NY, USA). The culture media were supplemented with 10% fetal bovine serum and antibiotics (50 units/ml penicillin, and 50 μg/ml streptomycin, Gibco, Logan City, UT, USA).

MTT, EdU, invasion, and scratch assays

Cellular viability was examined using an MTT assay (Invitrogen, Carlsbad, CA, USA) with the procedure previously described (40), as well as an EdU assay with a fluorescence-based cell proliferation kit (Thermo-Fisher, Waltham, MA, USA). A Transwell invasion assay and a wound-healing scratch assay were conducted as described previously (41).

Western blotting, shRNA transfection, ELISA, and protein array analysis

We used antibodies against AANAT (ab3505), CD105 (ab54338) (Abcam, Cambridge, MA, USA), Lrp5 (5731s), Lrp6 (3395T), Runx2 (8486s), Snail (3879s) (Cell Signaling, Danvers, MA, USA), CSF1 (sc-365779), MMP9 (sc-393859), PPARγ (sc−7273) (Santa Cruz Biotechnology, Dallas, Texas, USA), Tyrosine Hydroxylase (NB300-109, Novus Biologicals, Centennial, CO, USA), and β-actin (A5441, Sigma, Saint Louis, MO, USA). We employed RNA interference to reduce the expression of Lrp5 and Lrp6 using shRNA (sc-149050-V, sc-149050-V, Santa Cruz).

The levels of cholesterol, dopamine, and melatonin in mouse urine were determined using ELISA kits (MyBioSource, San Diego, CA, USA), and their concentrations were normalized per unit urinary volume. We also employed a proteome profiler human XL cytokine array kit (R&D Systems, Minneapolis, MN, USA) and determined expression of 105 cytokines and chemokines in human urine samples.

FRET imaging

To evaluate tension force at a focal adhesion and migratory capacity of tumor cells, a plasmid expressing a vinculin tension sensor (VinTS, #26019, Addgene, Watertown, MA, USA) was transfected and the fluorescence efficiency images were acquired by a custom-made microscope built on a laser scanning confocal microscope (FluoView 1000, Olympus; Center Valley, PA, USA) (32). Of note, an elevation in the tension force of the vinculin sensor implies a decrease in FRET efficiency.

Analysis of VOCs

From C57BL/6/c mice, 40 urine samples (50 μl) were collected before tibia loading, and 1 or 2 h after tibia loading. VOCs were analyzed by solid-phase microextraction coupled with gas chromatography-mass spectrometry (42). Hierarchical heatmap analysis was conducted for six compounds, which were statistically significant with the lowest p-value (Student's t-test) in the two groups before and after loading. Principal component analysis of all samples and the six VOCs was performed. Box and whisker plots for the two significantly upregulated VOCs were produced using Origin (OriginLab 2018, Northampton, MA, USA).

Gene expression profiling interactive analysis (GEPIA)

Using a GEPIA server (43) for accessing TCGA (The Cancer Genome Atlas) and GTEx (Genotype-Tissue Expression) datasets, the correlation coefficient for the mRNA levels in 6 gene pairs was obtained in the muscle-skeletal system. Data are given on a logarithmic scale (base 2) with a unit of transcript per million (TPM). Furthermore, the survival rates for patients with breast, prostate and pancreatic cancers were obtained for the high (top 75%) and low (bottom 25%) levels of the selected genes (Lrp5, CSF1, and CD105).

Statistical analysis

Three or four independent experiments were conducted and data were expressed as mean ± S.D. The sample size for evaluating mammary tumors in the mouse model was chosen to achieve a power of 80% with $p < 0.05$. Statistical significance was evaluated using a one-way analysis of variance (ANOVA). Post hoc statistical comparisons with control groups were performed using Bonferroni correction with statistical significance at $p < 0.05$. The single, double or triple asterisks indicate $p < 0.05$, $p < 0.01$, $p < 0.001$, respectively.

Results

Inhibitory effects of loading-conditioned urine medium (UM) on tumor cells

Urine samples were collected from C57BL/6 female mice before and 1 h after 5 N tibial loading (Fig. 1a). The media containing 0.1 to 3% urine, collected prior to tibia loading, did not significantly alter MTT-based cellular viability (Suppl. Fig. S1a). Hereafter, we employed UM consisting of 2% urine. While unconditioned UM did not alter cellular viability, loading-conditioned UM reduced it (Fig. 1b). An EdU assay showed that loading-conditioned UM decreased tumor cell proliferation but not unconditioned UM (Fig. 1c&d). Cellular invasion and migration were significantly reduced by loading-conditioned UM (Fig. 1e-h). Furthermore, the levels of Lrp5, Snail, MMP9, PPARγ, and Runx2 were downregulated by loading-conditioned UM but not by unconditioned UM (Fig. 1i&j). The level of Lrp6 was unchanged by both UMs. Of note, no significant difference in pH was observed in urine samples (Suppl. Fig. S1b). Notably, the tumor-suppressing effects of loading-conditioned UM were also observed in human prostate and pancreatic cancer cell lines (Suppl. Fig. S1c-h).

Loading-driven regulation of cholesterol, dopamine, and melatonin in urine

To investigate the potential mechanism of the tumor-suppressing capability, we conducted an ELISA assay focusing on cholesterol, dopamine, and melatonin. We observed that, compared to unconditioned urine, loading-derived urine lowered the level of cholesterol and elevated the levels of dopamine and melatonin (Fig. 2a-c). We then examined the effect of these three compounds on proliferation and invasion of EO771 tumor cells. MTT-based cellular viability and cellular proliferation showed that cholesterol promoted cellular growth, and dopamine and melatonin inhibited it (Fig. 2d&e). In the invasion assay, cholesterol stimulated invasion of

EO771 cells (Fig. 2f), by upregulating Lrp5, Snail, MMP9, PPARγ, and Runx2 (Fig. 2g). In contrast, dopamine and melatonin reduced cellular invasion and downregulated these genes (Fig. 2h-k). We also examined the effect of simvastatin and mevalonate. Simvastatin is an FDA-approved drug for reducing the risk of heart attack by blocking cholesterol synthesis, while mevalonate is a precursor necessary for synthesizing cholesterol. Administration of simvastatin reduced cellular invasion and downregulated Lrp5, Snail, MMP9, PPARγ, and Runx2 (Suppl. Fig. S2a-d). In contrast, the response to mevalonate was opposite, in which cellular invasion was elevated with an increase in these genes (Suppl. Fig. S2e-h).

Involvement of Lrp5 in anti-tumor effects by loading-conditioned UM

To evaluate the potential role of Lrp5 and Lrp6, we employed RNA interference. In response to the silencing of Lrp5, the cellular invasive capability was reduced in EO771 cells, but the silencing of Lrp6 did not significantly alter invasive capability (Fig. 3a). Also, the silencing of Lrp5 decreased Snail, MMP9, PPARγ, and Runx2 (Fig. 3b) and failed to retain the anti-tumor effects by loading-conditioned UM. Although Lrp6 silencing reduced MMP9 and PPARγ, it did not significantly alter the levels of Snail and Runx2 (Fig. 3c). Furthermore, Lrp5-deleted EO771 cells reduced cell viability and migration, but Lrp6-deleted EO771 cells did not (Fig. 3d&e).

Loading-driven alteration in urinary volatile organic compounds (VOCs)

We next examined any alteration of urinary VOCs due to skeletal loading and found a total of 106 VOCs that were detected in at least 50% of one sample class (loading or control). Fifteen of the 106 VOCs (about 14%) were identified to be differentially excreted with a p-value < 0.05 between loading and control samples. Among 9 unconditioned and 21 loading-conditioned urine

samples, hierarchical heatmap analysis highlighted 6 VOCs with the lowest p-values between the two sample groups (Fig. 3f; Table 1). Utilizing these VOCs were used to separate two groups of urine samples in a principal component plane (Fig. 3g). Principal component analysis of the six VOCs separated two ketones (upregulated by loading) and four esters (downregulated by loading) (Fig. 3h&i). Notably, incubation of hypothalamic neuronal cells with the two loading-enriched ketones elevated the level of aralkylamine N-acetyltransferase (AANAT) and tyrosine hydrogenase (TH) (Suppl. Fig. S3a) and reduced MMT-based tumor viability (Suppl. Fig. S3b-e). Of note, AANAT and TH are rate-limiting enzymes for the production of melatonin and dopamine, respectively.

Inhibition of tumor growth by loading-conditioned UM

To further examine the effect of loading-conditioned UM, we employed a mouse model of the mammary tumor and injected loading-conditioned UM into the tumor at the mammary fat pad (N = 12). Compared to the placebo control and unconditioned UM, loading-conditioned UM significantly reduced tumor size and weight (Fig. 4a).

Elevated TH and AANAT in the brain after tibia loading

Since a primary synthesis site of these neurotransmitters is the brain, we conducted immunohistochemistry. Compared to the staining of the placebo samples, the brain section of the loading group showed stronger staining of TH in the ventral tegmental area and AANAT in the pineal gland (Fig. 4b-e). Furthermore, Western blotting revealed that the levels of TH and AANAT were elevated in the brain by tibia loading (Fig. 4f).

Downregulation of CSF1 by loading-conditioned UM

CSF1 is a secreted cytokine that plays a role in the development of bone-resorbing osteoclasts and the progression of many cancers including breast cancer. In MDA-MB-231 and EO771 cells, the level of CSF1 was reduced by loading-conditioned UM (Fig. 4g). Also, the level of CSF1 was elevated by cholesterol, and reduced by dopamine and melatonin (Fig. 4h). Furthermore, CSF1 promoted the invasion and migration of MDA-MB-231 cells (Fig. 4j) and elevated the expression level of Lrp5, Snail, MMP9, Runx2, and PPARγ (Fig. 4k).

Inhibitory effects of human urine after step aerobics

Here, we also employed human urine collected before and 1 h after 30-min step aerobics. The result revealed that in 6 cancer cell lines, the urine sample after step aerobics reduced cellular viability (Fig. 5a&b). While the reduction was statistically significant in all cell lines, the largest reduction was observed in 4T1.2 tumor cells and the smallest in PC-3 prostate cancer cells. In response to one human sample (sample B in Fig. 5a) collected after step aerobics, MDA-MB-231 cells showed a decrease not only in MTT-based viability but also in cellular migration (Fig. 5c&d). However, no significant alterations were observed in response to the sample prior to step aerobics. Furthermore, aerobics-conditioned urine reduced the expression of Lrpt5, Snail, MMP9, PPARγ, and Runx2 and inhibited cellular invasion (Fig. 5e&f). No detectable changes were observed with unconditioned UM.

Elevation of FRET efficiency by weakening tensile force with post-aerobics urine

To examine the effect of cholesterol, dopamine, melatonin, and urine on tensile forces in focal adhesion sites that are necessary for cellular migration, we used a vinculin tension sensor and

evaluated molecular forces across focal adhesions. Compared with the control group, cholesterol in the medium lowered FRET efficiency, while dopamine, melatonin, and aerobics-conditioned UM elevated FRET efficiency (Fig. 5g). The observed elevation of FRET efficiency by dopamine and melatonin as well as aerobics-conditioned UM indicates that these agents weakened tensile forces at focal adhesions.

Differential expression of CD105 in urine samples before and after step aerobics

Besides cholesterol, dopamine, and melatonin, the protein array analysis revealed that three molecules (CD105, MIF, and Resistin) were downregulated in the urine after step aerobics (Fig. 6a), of which the change in CD105 was most significant. When MDA-MB-231 and PC-3 cancer cells were treated with the human urine, the level of CD105 was reduced by aerobics-conditioned UM (Fig. 6b). In response to treatment with CD105, Lrp5, Snail, MMP9, and Runx2 were upregulated (Fig. 6c). Consistent with the actions of tumor-stimulating cholesterol, CD105 was elevated by incubation with cholesterol (Fig. 6d). In contrast, dopamine and melatonin downregulated CD105 (Fig. 6d). Furthermore, the silencing of Lrp5 reduced CD105 and incubation with CSF1 elevated CD105 (Fig. 6e).

Linkage to transcript profiles and survival rates in TCGA and GTEx datasets

Using a GEPIA server, we lastly consulted with TCGA and GTEx datasets and analyzed gene expression levels of the key regulatory factors and their influence on survival rates of cancer patients. The correlation analysis among 7 genes (Lrp5, CSF1, CD105, Runx2, MMP9, PPARγ, and Snail) gave Pearson's coefficients larger than 0.32 for 6 pairs (Fig. 7a). For instance, the correlation coefficient was 0.65 for a pair of (Lrp5, CSF1) and (CD105, PPARγ). Regarding the

overall survival rate in patients with breast, prostate and pancreatic cancers, the high levels of Lrp5, CSF1, and CD105 showed a survival rate significantly lower than their low-level counterparts (Fig. 7b).

Discussion

This study presents *in vitro* and *in vivo* anti-tumor capability of mouse and human urine after physical activity. We observed the suppression of tumor progression not only with loading-conditioned UM in the mouse model but also aerobics-conditioned human UM. In the mouse model, tibia loading elevated tumor-suppressive dopamine and melatonin in the urine, with a reduction in tumor-promoting cholesterol. The signaling analysis revealed that dopamine and melatonin downregulated Lrp5, a co-receptor of Wnt signaling that stimulates tumor progression, while cholesterol upregulated it. Consistent with the effect of urine on Lrp5, a silencing of Lrp5 inhibited tumor-promoting genes such as Snail, MMP9, and Runx2 in EO771 and MDA-MB-231 cells. Furthermore, urine's anti-tumor capability was observed not only in breast cancer cells but also in cells derived from prostate and pancreatic cancers.

The loading-driven regulation of dopamine and melatonin is not well understood. Dopamine is synthesized in the ventral tegmental area as a neurotransmitter that primarily regulates motor control and motivation (44), while melatonin is secreted from the pineal gland and acts as an antioxidant as well as a sleep aid (45). The association of dopamine with physical activity is reported in rat studies (25, 26), and physical activity is also known to increase melatonin in serum (27, 28). While an elevated melatonin level in urine is reported to reduce cancer risks in breast, prostate, and bladder (46-48), the linkage of urinary dopamine to any cancer has not been reported. In the present mouse study, it is possible that locally applied mechanical stimulation is transmitted to the brain via neuronal signaling, and/or endocrine signaling through blood circulation. Further analysis is needed to determine the loading-driven regulatory mechanism to

the ventral tegmental area and the pineal gland, as well as the most appropriate loading conditions for regulating dopamine and melatonin.

Urinary VOC analysis via hierarchical clustering and principal component analysis revealed that tibia loading downregulated volatile esters and upregulated ketones. Interestingly, dibutyl phthalate, one of the downregulated esters, was reported as a ligand for melatonin receptors (49). In contrast, ketogenic metabolism was reported to stimulate dopamine synthesis (50, 51). We also observed that, in hypothalamic neuronal cells, the two loading-enriched ketones elevated levels of AANAT and TH, the rate-limiting enzymes for the production of melatonin and dopamine, respectively. This *in vitro* result complements the urinary VOC analysis, suggesting that the two ketones may potentially upregulate the production of dopamine and melatonin *in vivo*.

Besides load-driven regulation of dopamine and melatonin, ELISA revealed the involvement of cholesterol in urine's anti-tumor capability. The ELISA-based urinary cholesterol level was decreased approximately by 40% after skeletal loading in mice. Cholesterol is synthesized via the mevalonate pathway, in which simvastatin and mevalonate act as an inhibitor and stimulator, respectively (52). As analyzed *in vitro*, simvastatin-driven downregulation of MMP9, Snail, and PPARγ in E0771 and MDA-MB-231 cells was suppressed by mevalonate. Mevalonate is an intermediate product leading to cholesterol synthesis, and the observed mevalonate effect is consistent with our previous study focusing on pitavastatin, another inhibitor of the mevalonate pathway (53).

Since Wnt signaling is reported to promote tumor progression, the downregulation of Lrp5, a co-receptor of Wnt signaling, by loading-conditioned UM is in good agreement with its anti-tumor capability (Fig. 7c). Most notably, the present result showed that the anti-tumor effect was suppressed by silencing Lrp5 and not Lrp6, indicating that urine's anti-tumor capability is mediated by Lrp5. A linkage of Lrp5 to serotonin has been reported, in which mice carrying a conditional deletion of Lrp5 increased serotonin in the serum (54). To our knowledge, however, it has been shown for the first time that dopamine and melatonin downregulate Lrp5 in tumor cells. Protein array analysis revealed that CD105 (also known as Endoglin) was significantly reduced by step aerobics-conditioned human urine sample, and it is downstream of Lrp5 and CSF1. CD105 is part of the TGFβ receptor complex and involved in tumor-related angiogenesis (55). CSF1 is a hematopoietic growth factor and is linked to bone homeostasis and progression of many cancers including breast cancer (30).

TCGA data for breast, prostate, and pancreatic cancers revealed that the overall survival rates were significantly lowered for the patients with a high level of Lrp5, CSF1 or CD105 than those with a low level. Furthermore, the positive correlations in GTEx data were observed among the regulatory genes in Fig. 7c, especially for the pairs of (Lrp5, CSF1), (CD105, PPARγ) and (CSF1, CD105). These clinical data further support the significance of the urine's anti-tumor capability with the proposed regulatory mechanism.

Urine can be used as a diagnostic agent for bladder-linked diseases (56, 57), and it also serves as a non-invasive biomarker in sport and exercise medicine (58). However, its potential use for cancer detection and treatment is not well established. In this study, we showed the critical role

of physical activity in regulating urine compositions. Notably, urine collected prior to loading or step aerobics did not alter the proliferation and migration of cancer cells or the growth of tumors, suggesting that physical activities are essential to convert urine into an anti-tumor agent. While the present results reveal a novel possibility of urine's use, the study has a few limitations. Besides step aerobics, it is important to evaluate the potential benefits of other physical activities such as walking, swimming, and stretching. While Lrp5-CSF1-CD105 signaling was shown to induce the anti-tumor action *in vitro*, its role *in vivo* needs to be investigated. The urinary concentrations of cholesterol, dopamine, and melatonin can be normalized by the creatinine concentration. We employed breast-cancer cell lines, as well as prostate and pancreatic cancer cell lines. It is possible that sensitivity depends on the types of cancer cells.

In summary, this study revealed that a relatively short period (5 to 10 min) of medium-level loading converted urine into a markedly effective anti-tumor biofluid. It has been shown for the first time that 5-min tibia loading or 30-min step aerobics is sufficient to sharply alter the levels of cholesterol, dopamine, and melatonin in urine, and downregulate the tumor-promoting genes such as Lrp5, CSF1, and CD105. Because of the high survival rate for patients with a low transcript level in the Lrp5-CSF1-CD105 regulatory axis, this study indicates a dual role of loading-conditioned urine as a potential tumor suppressor and a source of diagnostic biomarkers.

Acknowledgments

The authors appreciate Mengdi Zhang for preparing FRET tension sensor plasmids, and Chuanpeng Dong and Yunlong Liu for bioinformatics analysis. This study was in part supported by NIH R01 AR52144 and R03 CA238555 (HY).

Author Contributions

J. Liu, M. Agarwal, B.-Y. Li and H. Yokota designed the study; D. Wu, Y. Fan, S. Liu, MD. Woollam, X. Sun, E. Murao, R. Zha, C. Park, AP. Siegel collected and interpreted data; D. Wu, MD. Woollam, R. Prakash, B.-Y. Li and H. Yokota drafted the manuscript; and all authors reviewed the manuscript and approved the final draft.

References

1. Savica, V., Calo, L. A., Santoro, D., Monardo, P., Mallamace, A., and Bellinghieri, G. (2011) Urine therapy through the centuries. *J Nephrol* **24 Suppl 17**, S123-125
2. Rastogi, S., and Kaphle, K. (2011) Sustainable traditional medicine: taking the inspirations from ancient veterinary science. Evid Based Complement *Alternat Med* **2011**, 151435
3. Armstrong, J. A. (2007) Urinalysis in Western culture: a brief history. *Kidney Int* **71**, 384-387
4. Armstrong, J. A. (1971) The Water of Life: A Treatise on Urine Therapy., The C.W. Daniel Company Ltd, United Kingdom
5. Gogtay, N. J., Bhatt, H. A., Dalvi, S. S., and Kshirsagar, N. A. (2002) The use and safety of non-allopathic Indian medicines. *Drug Saf* **25**, 1005-1019
6. Bower, J. E., Ganz, P. A., Desmond, K. A., Rowland, J. H., Meyerowitz, B. E., and Belin, T. R. (2000) Fatigue in breast cancer survivors: occurrence, correlates, and impact on quality of life. *J Clin Oncol* **18**, 743-753
7. Nayak, M. G., George, A., Vidyasagar, M. S., Mathew, S., Nayak, S., Nayak, B. S., Shashidhara, Y. N., and Kamath, A. (2015) Symptoms experienced by cancer patients and barriers to symptom management. *Indian J Palliat Care* **21**, 349-354
8. Romli, F., Abu, N., Khorshid, F. A., Syed Najmuddin, S. U. F., Keong, Y. S., Mohamad, N. E., Hamid, M., Alitheen, N. B., and Nik Abd Rahman, N. M. A. (2017) The Growth Inhibitory Potential and Antimetastatic Effect of Camel Urine on Breast Cancer Cells In Vitro and In Vivo. *Integr Cancer Ther* **16**, 540-555
9. Vaidya, A. D. B. (2018) Urine therapy in Ayurveda: Ancient insights to modern discoveries for cancer regression. *J Ayurveda Integr Med* **9**, 221-224
10. Bouatra, S., Aziat, F., Mandal, R., Guo, A. C., Wilson, M. R., Knox, C., Bjorndahl, T. C., Krishnamurthy, R., Saleem, F., Liu, P., Dame, Z. T., Poelzer, J., Huynh, J., Yallou, F. S., Psychogios, N., Dong, E., Bogumil, R., Roehring, C., and Wishart, D. S. (2013) The human urine metabolome. *PLoS One* **8**, e73076
11. Warburton, D. E., Nicol, C. W., and Bredin, S. S. (2006) Health benefits of physical activity: the evidence. *CMAJ* **174**, 801-809
12. Ruegsegger, G. N., and Booth, F. W. (2018) Health Benefits of Exercise. *Cold Spring Harb Perspect Med* **8**
13. Pedersen, B. K., and Saltin, B. (2015) Exercise as medicine - evidence for prescribing exercise as therapy in 26 different chronic diseases. *Scand J Med Sci Sports* **25 Suppl 3**, 1-72
14. Segal, R., Zwaal, C., Green, E., Tomasone, J. R., Loblaw, A., Petrella, T., and Exercise for People with Cancer Guideline Development, G. (2017) Exercise for people with cancer: a systematic review. *Curr Oncol* **24**, e290-e315
15. Ji, L. L., Gomez-Cabrera, M. C., and Vina, J. (2006) Exercise and hormesis: activation of cellular antioxidant signaling pathway. *Ann N Y Acad Sci* **1067**, 425-435
16. Rundqvist, H., Augsten, M., Stromberg, A., Rullman, E., Mijwel, S., Kharaziha, P., Panaretakis, T., Gustafsson, T., and Ostman, A. (2013) Effect of acute exercise on prostate cancer cell growth. *PLoS One* **8**, e67579
17. Dethlefsen, C., Lillelund, C., Midtgaard, J., Andersen, C., Pedersen, B. K., Christensen, J. F., and Hojman, P. (2016) Exercise regulates breast cancer cell viability: systemic training adaptations versus acute exercise responses. *Breast Cancer Res Treat* **159**, 469-479

18. Dethlefsen, C., Pedersen, K. S., and Hojman, P. (2017) Every exercise bout matters: linking systemic exercise responses to breast cancer control. *Breast Cancer Res Treat* **162**, 399-408
19. Dethlefsen, C., Hansen, L. S., Lillelund, C., Andersen, C., Gehl, J., Christensen, J. F., Pedersen, B. K., and Hojman, P. (2017) Exercise-Induced Catecholamines Activate the Hippo Tumor Suppressor Pathway to Reduce Risks of Breast Cancer Development. *Cancer Res* **77**, 4894-4904
20. Picke, A. K., Sylow, L., Moller, L. L. V., Kjobsted, R., Schmidt, F. N., Steejn, M. W., Salbach-Hirsch, J., Hofbauer, C., Bluher, M., Saalbach, A., Busse, B., Rauner, M., and Hofbauer, L. C. (2018) Differential effects of high-fat diet and exercise training on bone and energy metabolism. *Bone* **116**, 120-134
21. Liao, H. W., Huang, T. H., Chang, Y. H., Liou, H. H., Chou, Y. H., Sue, Y. M., Hung, P. H., Chang, Y. T., Ho, P. C., and Tsai, K. J. (2019) Exercise Alleviates Osteoporosis in Rats with Mild Chronic Kidney Disease by Decreasing Sclerostin Production. *Int J Mol Sci* **20**
22. Muzio, L., Brambilla, V., Calcaterra, L., D'Adamo, P., Martino, G., and Benedetti, F. (2016) Increased neuroplasticity and hippocampal microglia activation in a mice model of rapid antidepressant treatment. *Behav Brain Res* **311**, 392-402
23. Stranahan, A. M., Lee, K., Becker, K. G., Zhang, Y., Maudsley, S., Martin, B., Cutler, R. G., and Mattson, M. P. (2010) Hippocampal gene expression patterns underlying the enhancement of memory by running in aged mice. *Neurobiol Aging* **31**, 1937-1949
24. Feng, X., Zhang, L., Xu, S., and Shen, A. Z. (2019) ATP-citrate lyase (ACLY) in lipid metabolism and atherosclerosis: An updated review. *Prog Lipid Res* **77**, 101006
25. Gerald, M. C. (1978) Effects of (+)-amphetamine on the treadmill endurance performance of rats. *Neuropharmacology* **17**, 703-704
26. Heyes, M. P., Garnett, E. S., and Coates, G. (1985) Central dopaminergic activity influences rat's ability to exercise. *Life Sci* **36**, 671-677
27. Jing, H. F., and Wang, X. M. (2017) Effects of aerobic exercise combined with melatonin on osteoporosis of type II diabetic rats. *Zhongguo Ying Yong Sheng Li Xue Za Zhi* **33**, 252-256
28. Qiu, F., Liu, X., Zhang, Y., Wu, Y., Xiao, D., and Shi, L. (2018) Aerobic exercise enhanced endothelium-dependent vasorelaxation in mesenteric arteries in spontaneously hypertensive rats: the role of melatonin. *Hypertens Res* **41**, 718-729
29. Anastas, J. N., and Moon, R. T. (2013) WNT signalling pathways as therapeutic targets in cancer. *Nat Rev Cancer* **13**, 11-26
30. Chen, X., Ouyang, Z., Shen, Y., Liu, B., Zhang, Q., Wan, L., Yin, Z., Zhu, W., Li, S., and Peng, D. (2019) CircRNA_28313/miR-195a/CSF1 axis modulates osteoclast differentiation to affect OVX-induced bone absorption in mice. *RNA Biol* **16**, 1249-1262
31. Grashoff, C., Hoffman, B. D., Brenner, M. D., Zhou, R., Parsons, M., Yang, M. T., McLean, M. A., Sligar, S. G., Chen, C. S., Ha, T., and Schwartz, M. A. (2010) Measuring mechanical tension across vinculin reveals regulation of focal adhesion dynamics. *Nature* **466**, 263-266
32. Li, F., Chen, A., Reeser, A., Wang, Y., Fan, Y., Liu, S., Zhao, X., Prakash, R., Kota, D., Li, B. Y., Yokota, H., and Liu, J. (2019) Vinculin Force Sensor Detects Tumor-Osteocyte Interactions. *Sci Rep* **9**, 5615
33. Niziolek, P. J., Warman, M. L., and Robling, A. G. (2012) Mechanotransduction in bone tissue: The A214V and G171V mutations in Lrp5 enhance load-induced osteogenesis in a surface-selective manner. *Bone* **51**, 459-465

34. Fan, Y., Jalali, A., Chen, A., Zhao, X., Liu, S., Teli, M., Guo, Y., Li, J., Siegel, A., Yang, L., Liu, J., Na, S., Agarwal, M., Robling, A.G., Nakshatri, H., Li, B.Y., Yokota, H. (2020) Skeletal loading regulates breast cancer-associated osteolysis in a loading intensity-dependent fashion. *Bone Res*. https:/doi.org/10.1038/s41413-020-0083-6.
35. Ewens, A., Mihich, E., and Ehrke, M. J. (2005) Distant metastasis from subcutaneously grown E0771 medullary breast adenocarcinoma. *Anticancer Re*s **25**, 3905-3915
36. Lelekakis, M., Moseley, J. M., Martin, T. J., Hards, D., Williams, E., Ho, P., Lowen, D., Javni, J., Miller, F. R., Slavin, J., and Anderson, R. L. (1999) A novel orthotopic model of breast cancer metastasis to bone. *Clin Exp Metastasis* **17**, 163-170
37. Chen, A., Wang, L., Liu, S., Wang, Y., Liu, Y., Wang, M., Nakshatri, H., Li, B. Y., and Yokota, H. (2018) Attraction and Compaction of Migratory Breast Cancer Cells by Bone Matrix Proteins through Tumor-Osteocyte Interactions. *Sci Rep* **8**, 5420
38. Tai, S., Sun, Y., Squires, J. M., Zhang, H., Oh, W. K., Liang, C. Z., and Huang, J. (2011) PC3 is a cell line characteristic of prostatic small cell carcinoma. *Prostate* **71**, 1668-1679
39. Lieber, M., Mazzetta, J., Nelson-Rees, W., Kaplan, M., and Todaro, G. (1975) Establishment of a continuous tumor-cell line (panc-1) from a human carcinoma of the exocrine pancreas. *Int J Cancer* **15**, 741-747
40. Wang, L., Wang, Y., Chen, A., Jalali, A., Liu, S., Guo, Y., Na, S., Nakshatri, H., Li, B. Y., and Yokota, H. (2018) Effects of a checkpoint kinase inhibitor, AZD7762, on tumor suppression and bone remodeling. *Int J Oncol* **53**, 1001-1012
41. Xu, W., Wan, Q., Na, S., Yokota, H., Yan, J. L., and Hamamura, K. (2015) Suppressed invasive and migratory behaviors of SW1353 chondrosarcoma cells through the regulation of Src, Rac1 GTPase, and MMP13. *Cell Signa*l **27**, 2332-2342
42. Woollam, M., Teli, M., Angarita-Rivera, P., Liu, S., Siegel, A. P., Yokota, H., and Agarwal, M. (2019) Detection of Volatile Organic Compounds (VOCs) in Urine via Gas Chromatography-Mass Spectrometry QTOF to Differentiate Between Localized and Metastatic Models of Breast Cancer. *Sci Rep* **9**, 2526
43. Tang, Z., Li, C., Kang, B., Gao, G., Li, C., and Zhang, Z. (2017) GEPIA: a web server for cancer and normal gene expression profiling and interactive analyses. *Nucleic Acids Res* **45**, W98-W102
44. Runegaard, A. H., Fitzpatrick, C. M., Woldbye, D. P. D., Andreasen, J. T., Sorensen, A. T., and Gether, U. (2019) Modulating Dopamine Signaling and Behavior with Chemogenetics: Concepts, Progress, and Challenges. *Pharmacol Rev* **71**, 123-156
45. Ma, N., Zhang, J., Reiter, R. J., and Ma, X. (2019) Melatonin mediates mucosal immune cells, microbial metabolism, and rhythm crosstalk: A therapeutic target to reduce intestinal inflammation. *Med Res Rev* **40**, 606-632
46. Schernhammer, E. S., and Hankinson, S. E. (2005) Urinary melatonin levels and breast cancer risk. J Natl *Cancer Inst* **97**, 1084-1087
47. Tai, S. Y., Huang, S. P., Bao, B. Y., and Wu, M. T. (2016) Urinary melatonin-sulfate/cortisol ratio and the presence of prostate cancer: A case-control study. *Sci Rep* **6**, 29606
48. Watanabe, M. (2002) [Microanalysis of tryptophan metabolites and suppressor factor of delayed-type hypersensitivity in mice]. Yakugaku Zasshi **122**, 429-434
49. Anthony J Jones, M. L. D., and Rajendram V Rajnarayanan. (2017) Environmental Phthalate Diesters as hMT1 and hMT2 Melatonin Receptor Ligands. *FASEB JOURNAL* **31**
50. Cheng, B., Yang, X., An, L., Gao, B., Liu, X., and Liu, S. (2009) Ketogenic diet protects

dopaminergic neurons against 6-OHDA neurotoxicity via up-regulating glutathione in a rat model of Parkinson's disease. *Brain Res* **1286**, 25-31
51. Church, W. H., Adams, R. E., and Wyss, L. S. (2014) Ketogenic diet alters dopaminergic activity in the mouse cortex. *Neurosci Lett* **571**, 1-4
52. Wong, W. W., Dimitroulakos, J., Minden, M. D., and Penn, L. Z. (2002) HMG-CoA reductase inhibitors and the malignant cell: the statin family of drugs as triggers of tumor-specific apoptosis. *Leukemia* **16**, 508-519
53. Wang, L., Wang, Y., Chen, A., Teli, M., Kondo, R., Jalali, A., Fan, Y., Liu, S., Zhao, X., Siegel, A., Minami, K., Agarwal, M., Li, B. Y., and Yokota, H. (2019) Pitavastatin slows tumor progression and alters urine-derived volatile organic compounds through the mevalonate pathway. *FASEB J* **33**, 13710-13721
54. Yadav, V. K., Ryu, J. H., Suda, N., Tanaka, K. F., Gingrich, J. A., Schutz, G., Glorieux, F. H., Chiang, C. Y., Zajac, J. D., Insogna, K. L., Mann, J. J., Hen, R., Ducy, P., and Karsenty, G. (2008) Lrp5 controls bone formation by inhibiting serotonin synthesis in the duodenum. *Cell* **135**, 825-837
55. Kasprzak, A., and Adamek, A. (2018) Role of Endoglin (CD105) in the Progression of Hepatocellular Carcinoma and Anti-Angiogenic Therapy. *Int J Mol Sci* **19**, 3887
56. Kolouri, S., Daneshfard, B., Jaladat, A. M., and Tafazoli, V. (2017) Green Urine in Traditional Persian Medicine: Differential Diagnosis and Clinical Relevance. J Evid Based Complementary *Altern Med* **22**, 232-236
57. Becker, G. J., Garigali, G., and Fogazzi, G. B. (2016) Advances in Urine Microscopy. Am J *Kidney Dis* **67**, 954-964
58. Lindsay, A., and Costello, J. T. (2017) Realising the Potential of Urine and Saliva as Diagnostic Tools in Sport and Exercise Medicine. *Sports Med* **47**, 11-31

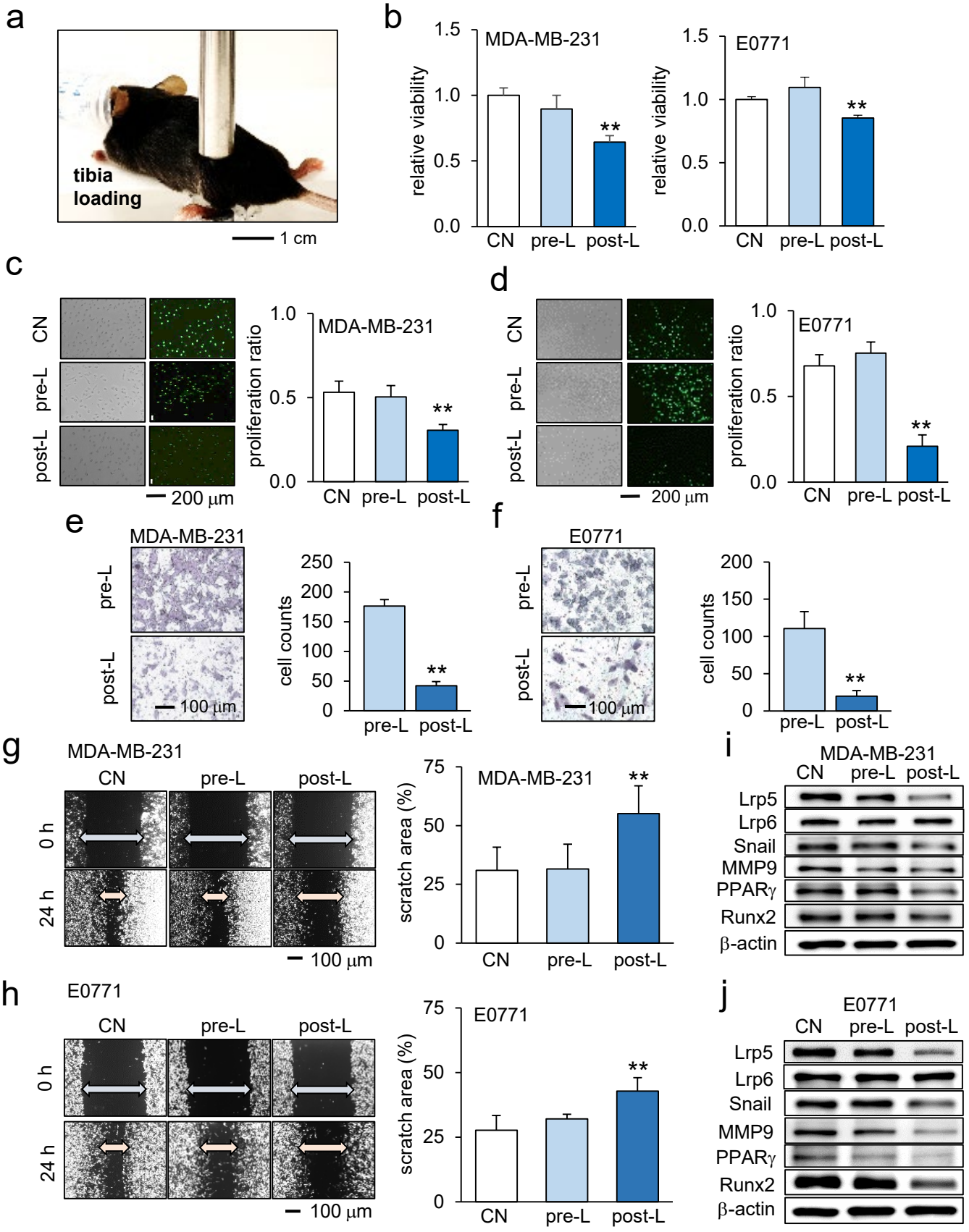
a
tibia loading
1 cm
b
MDA-MB-231
E0771
relative viability
1.5
1.0
0.5
0.0
**
CN
pre-L
post-L
c
d
CN
pre-L
post-L
200 μm
proliferation ratio
e
f
cell counts
250
200
150
100
50
0
100 μm
g
i
h
j
0 h
24 h
scratch area (%)
75
50
25
Lrp5
Lrp6
Snail
MMP9
PPARγ
Runx2
β-actin

Figure 1

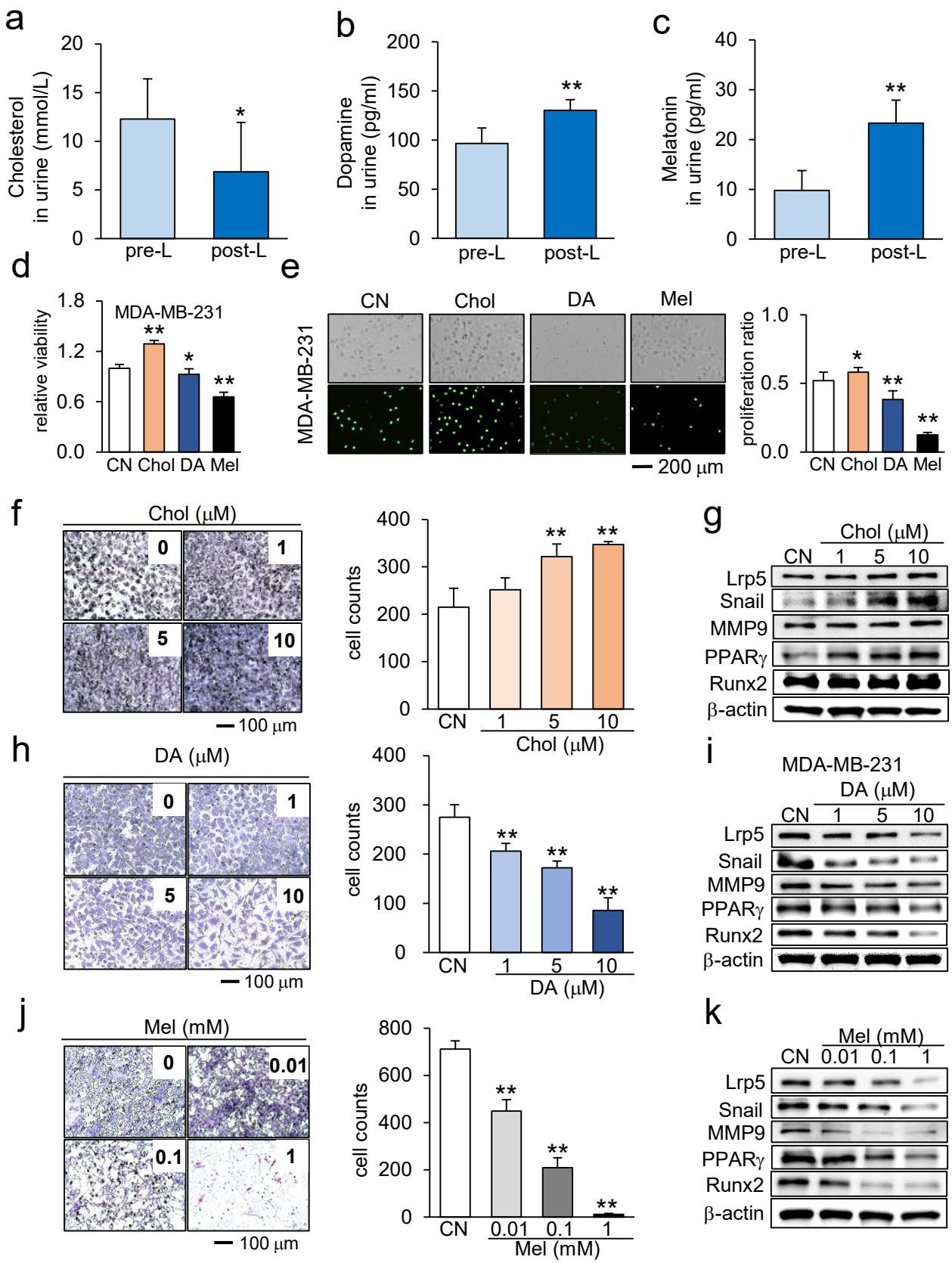
a
Cholesterol in urine (mmol/L)
pre-L
post-L
b
Dopamine in urine (pg/ml)
c
Melatonin in urine (pg/ml)
d
MDA-MB-231
relative viability
CN Chol DA Mel
e
CN Chol DA Mel
MDA-MB-231
200 μm
proliferation ratio
f
Chol (μM)
0 1 5 10
100 μm
cell counts
Chol (μM)
g
Chol (μM)
CN 1 5 10
Lrp5
Snail
MMP9
PPARγ
Runx2
β-actin
h
DA (μM)
DA (μM)
i
MDA-MB-231
DA (μM)
j
Mel (mM)
0 0.01 0.1 1
Mel (mM)
k
Mel (mM)

Figure 2

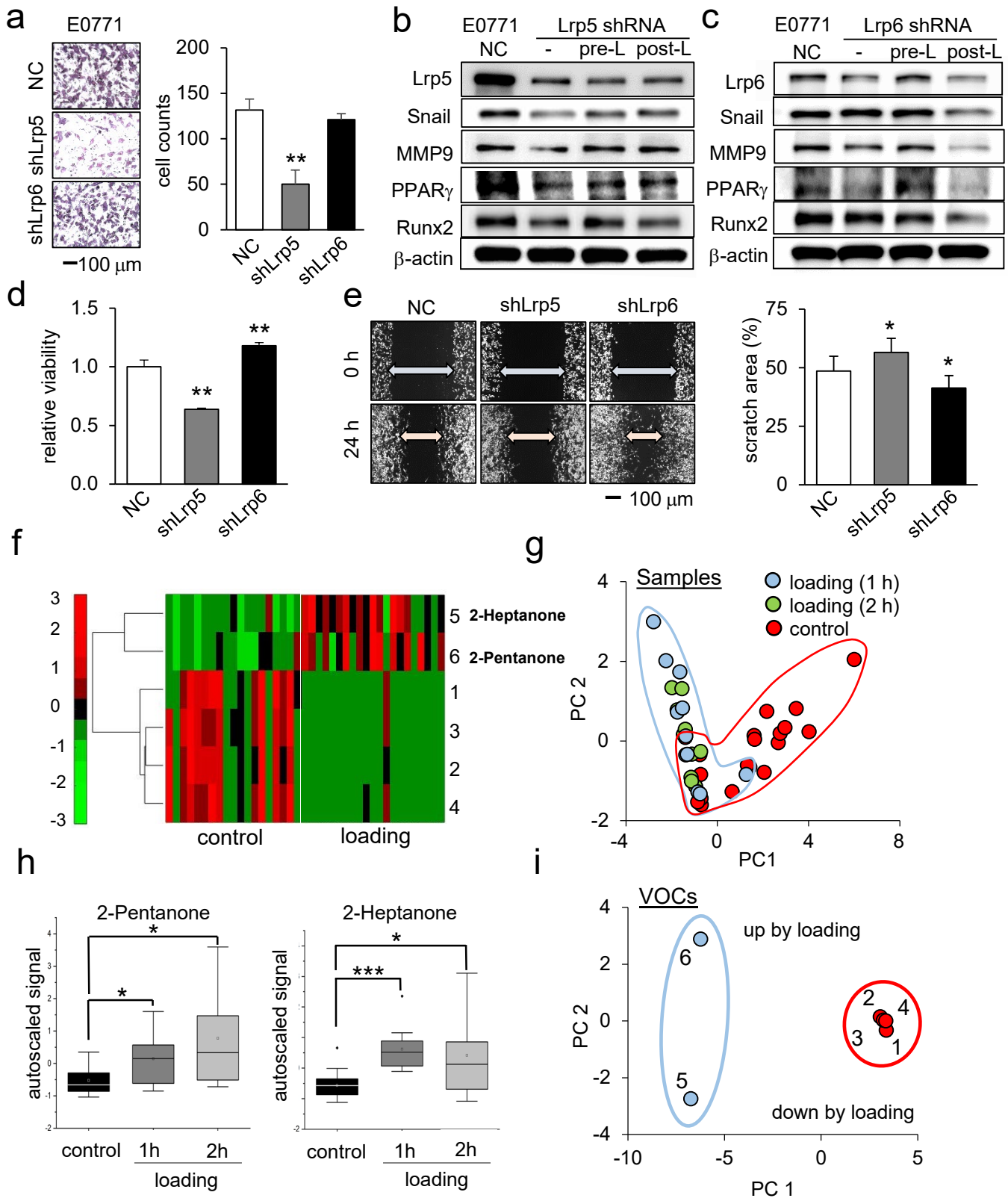
a
E0771
NC
shLrp5
shLrp6
100 μm
cell counts
200
150
100
50
0
**
NC
shLrp5
shLrp6
b
E0771
Lrp5 shRNA
NC
-
pre-L
post-L
Lrp5
Snail
MMP9
PPARγ
Runx2
β-actin
c
E0771
Lrp6 shRNA
NC
-
pre-L
post-L
Lrp6
Snail
MMP9
PPARγ
Runx2
β-actin
d
relative viability
1.5
1.0
0.5
0.0
**
**
NC
shLrp5
shLrp6
e
NC
shLrp5
shLrp6
0 h
24 h
100 μm
scratch area (%)
75
50
25
0
*
*
NC
shLrp5
shLrp6
f
3
2
1
0
-1
-2
-3
5 2-Heptanone
6 2-Pentanone
1
3
2
4
control
loading
g
Samples
loading (1 h)
loading (2 h)
control
PC 2
4
2
0
-2
-4
0
4
8
PC1
h
2-Pentanone
2-Heptanone
autoscaled signal
*
*
***
*
control
1h
2h
loading
i
VOCs
up by loading
down by loading
6
5
2
4
3
1
PC 2
PC 1
4
2
0
-2
-4
-10
-5
0
5

Figure 3

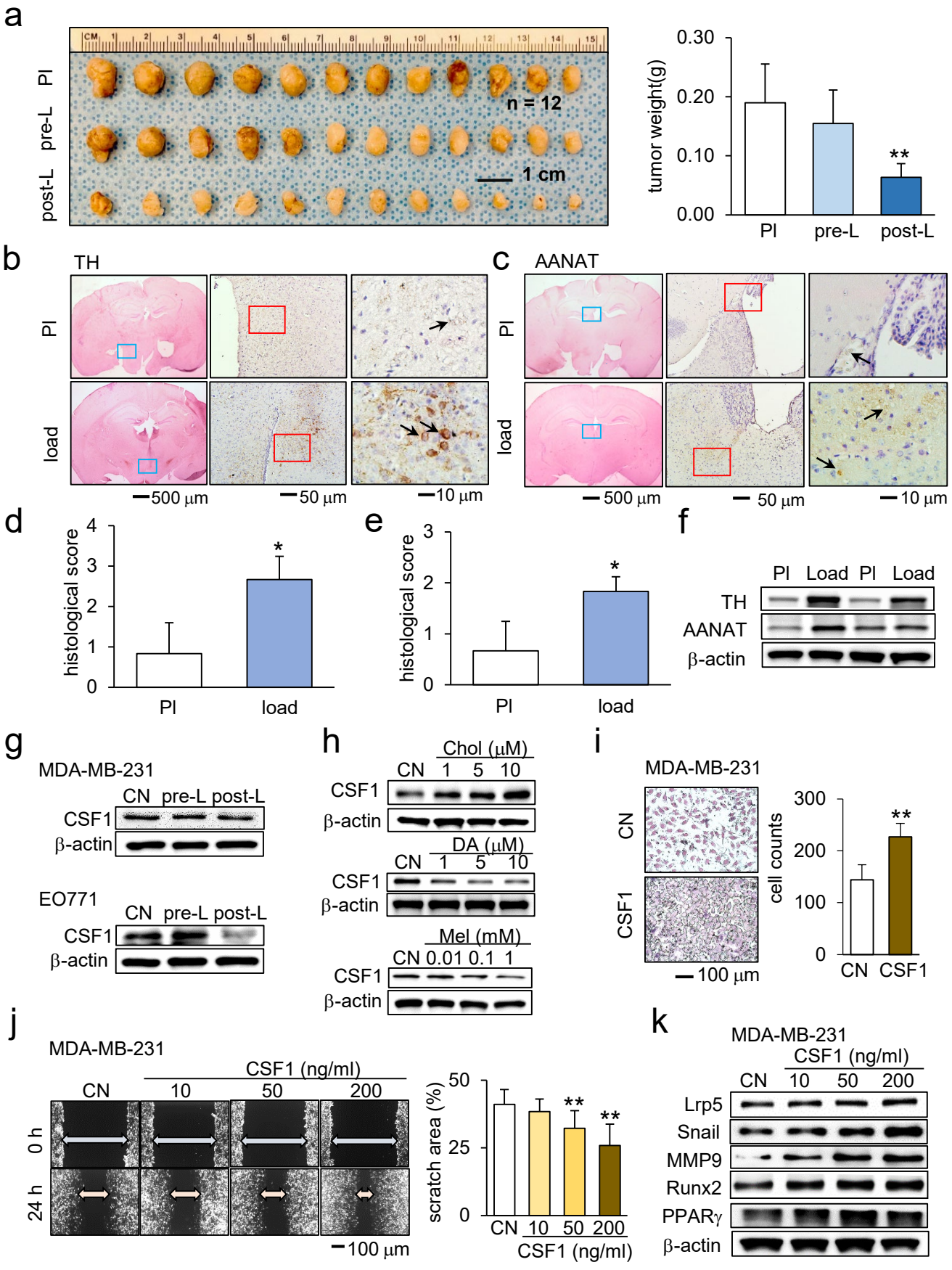
a
PI
pre-L
post-L
n = 12
1 cm
tumor weight(g)
0.30
0.20
0.10
0.00
**
PI
pre-L
post-L
b
TH
PI
load
500 μm
50 μm
10 μm
c
AANAT
PI
load
500 μm
50 μm
10 μm
d
histological score
4
3
2
1
0
*
PI
load
e
histological score
3
2
1
0
*
PI
load
f
PI Load PI Load
TH
AANAT
β-actin
g
MDA-MB-231
CN pre-L post-L
CSF1
β-actin
EO771
CN pre-L post-L
CSF1
β-actin
h
Chol (μM)
CN 1 5 10
CSF1
β-actin
DA (μM)
CN 1 5 10
CSF1
β-actin
Mel (mM)
CN 0.01 0.1 1
CSF1
β-actin
i
MDA-MB-231
CN
CSF1
100 μm
cell counts
300
200
100
0
**
CN CSF1
j
MDA-MB-231
CSF1 (ng/ml)
CN 10 50 200
0 h
24 h
100 μm
scratch area (%)
50
25
0
**
**
CN 10 50 200
CSF1 (ng/ml)
k
MDA-MB-231
CSF1 (ng/ml)
CN 10 50 200
Lrp5
Snail
MMP9
Runx2
PPARγ
β-actin

Figure 4

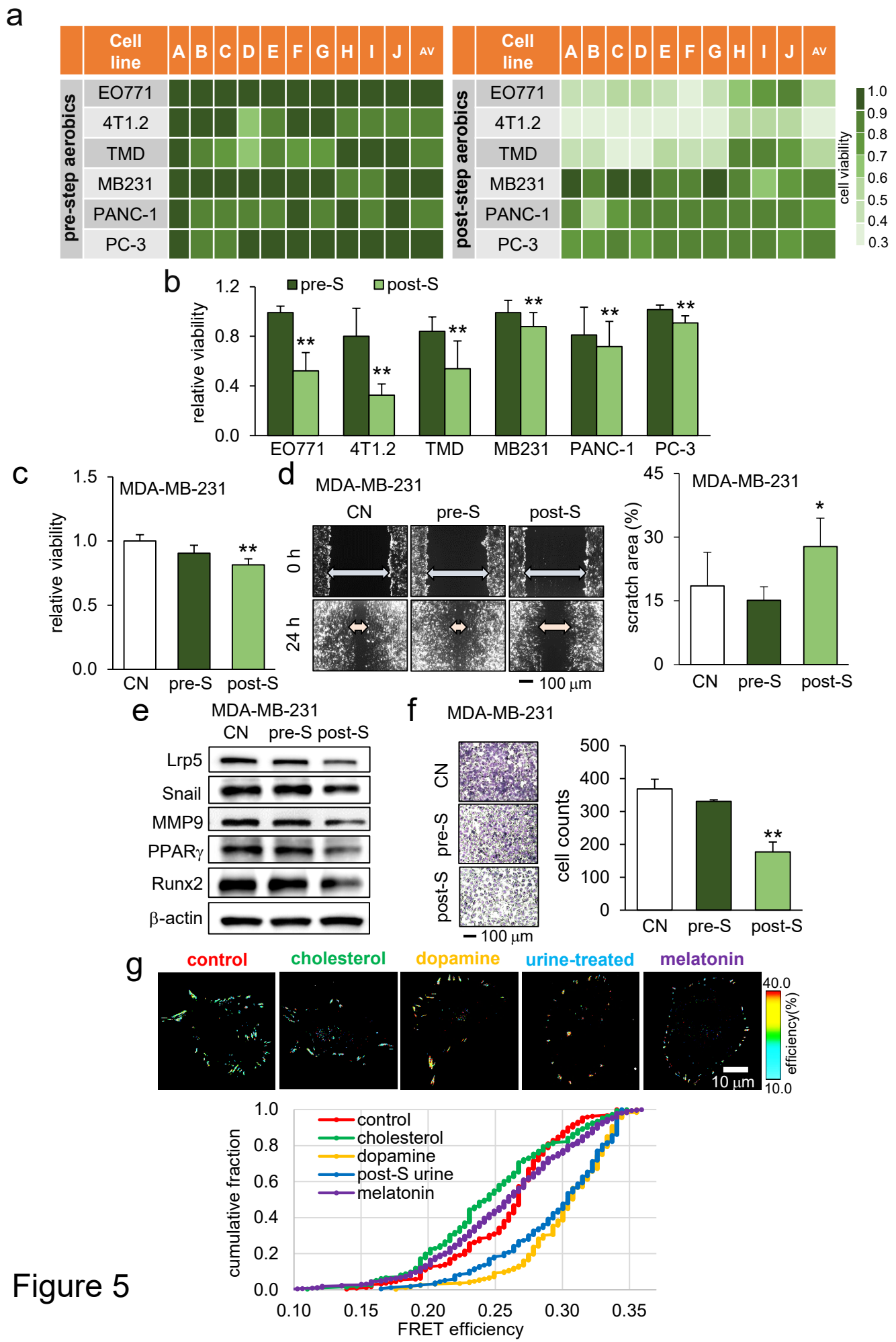
a
Cell line
A B C D E F G H I J AV
pre-step aerobics
post-step aerobics
EO771
4T1.2
TMD
MB231
PANC-1
PC-3
cell viability
1.0 0.9 0.8 0.7 0.6 0.5 0.4 0.3
b
pre-S
post-S
relative viability
1.2 0.8 0.4 0.0
**
EO771 4T1.2 TMD MB231 PANC-1 PC-3
c
MDA-MB-231
relative viability
1.5 1.0 0.5 0.0
**
CN pre-S post-S
d
MDA-MB-231
CN pre-S post-S
0 h
24 h
100 μm
scratch area (%)
45 30 15 0
*
e
MDA-MB-231
CN pre-S post-S
Lrp5
Snail
MMP9
PPARγ
Runx2
β-actin
f
MDA-MB-231
CN
pre-S
post-S
100 μm
cell counts
500 400 300 200 100 0
**
g
control
cholesterol
dopamine
urine-treated
melatonin
10 μm
efficiency(%)
40.0
10.0
cumulative fraction
1.0 0.8 0.6 0.4 0.2 0.0
control
cholesterol
dopamine
post-S urine
melatonin
0.10 0.15 0.20 0.25 0.30 0.35
FRET efficiency

Figure 5

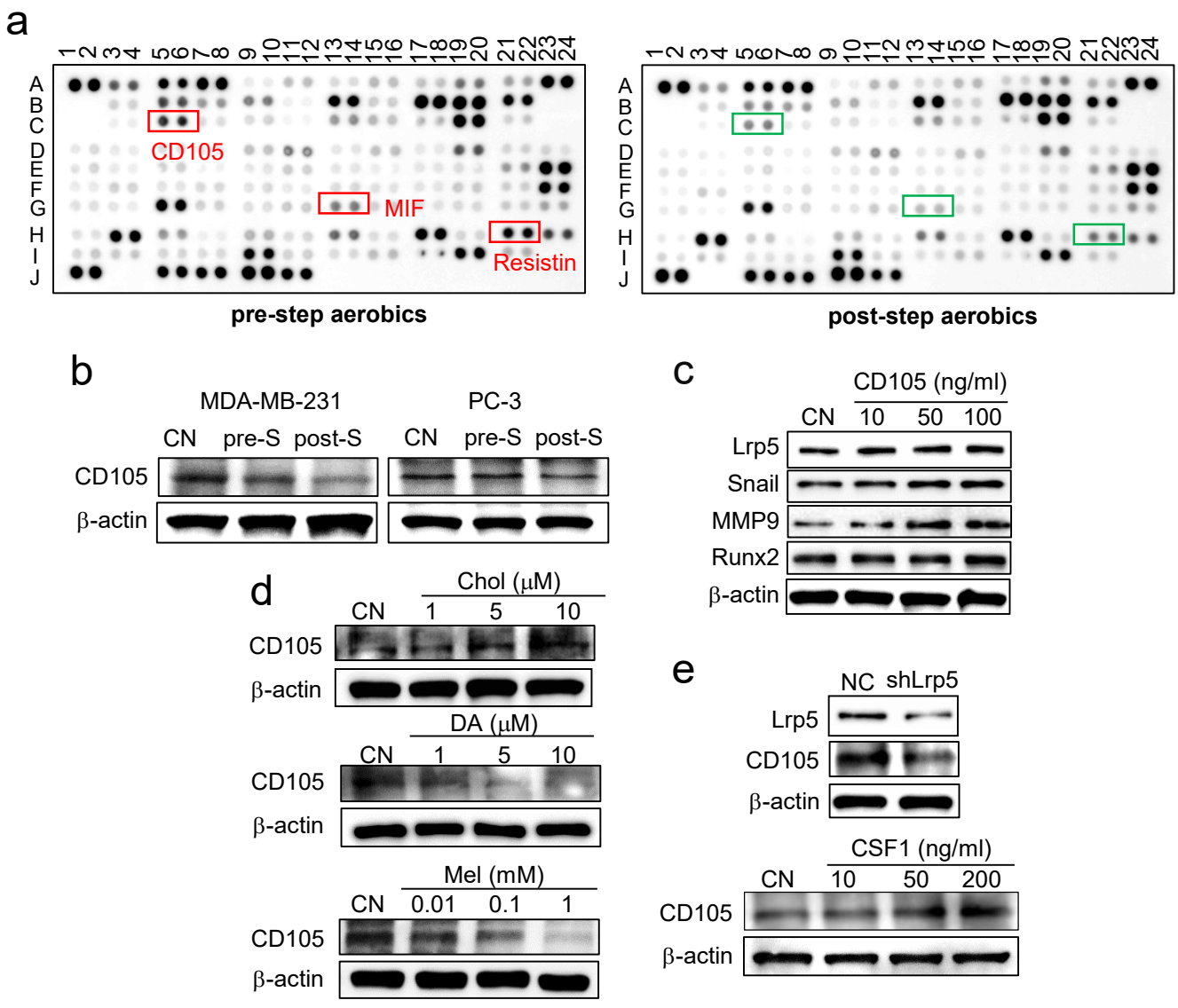
a
CD105
MIF
Resistin
pre-step aerobics
post-step aerobics
b
MDA-MB-231
PC-3
CN
pre-S
post-S
CD105
β-actin
c
CD105 (ng/ml)
CN
10
50
100
Lrp5
Snail
MMP9
Runx2
β-actin
d
Chol (μM)
DA (μM)
Mel (mM)
0.01
0.1
1
e
NC
shLrp5
CSF1 (ng/ml)
200

Figure 6

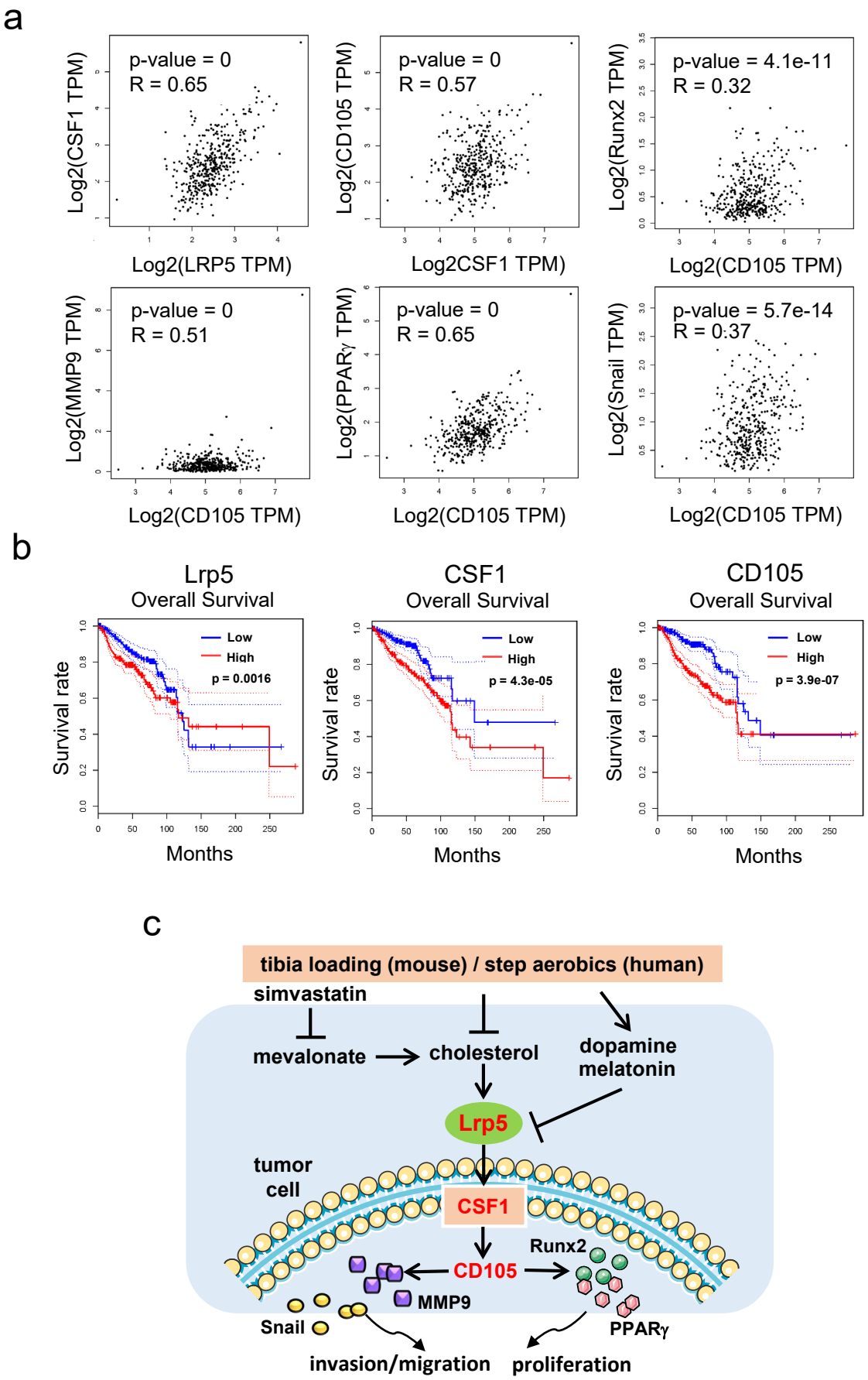
a
p-value = 0
R = 0.65
Log2(CSF1 TPM)
Log2(LRP5 TPM)
p-value = 0
R = 0.57
Log2(CD105 TPM)
Log2CSF1 TPM)
p-value = 4.1e-11
R = 0.32
Log2(Runx2 TPM)
Log2(CD105 TPM)
p-value = 0
R = 0.51
Log2(MMP9 TPM)
Log2(CD105 TPM)
p-value = 0
R = 0.65
Log2(PPARγ TPM)
Log2(CD105 TPM)
p-value = 5.7e-14
R = 0.37
Log2(Snail TPM)
Log2(CD105 TPM)
b
Lrp5
Overall Survival
Low
High
p = 0.0016
Survival rate
Months
CSF1
Overall Survival
Low
High
p = 4.3e-05
Survival rate
Months
CD105
Overall Survival
Low
High
p = 3.9e-07
Survival rate
Months
c
tibia loading (mouse) / step aerobics (human)
simvastatin
mevalonate
cholesterol
dopamine
melatonin
Lrp5
tumor
cell
CSF1
Runx2
CD105
MMP9
Snail
PPARγ
invasion/migration
proliferation

Figure 7

Supplementary Information

Loading-induced anti-tumor capability of murine and human urine

Supplementary Figure Legends

Suppl. Figure S1.
Effects of mouse urine on MDA-MB-231 breast cancer cells, EO771 mammary tumor cells, PC-3 prostate cancer cells, and PANC-1 pancreatic cancer cells. (a&b) No significant effect on MTT-based cellular viability by unconditioned UM. (b) pH of mouse urine. (c&d) Reduction in MTT-based cellular viability and migration by post-L urine in PC-3 cells. (e&f) Reduction in MTT-based cellular viability and migration by post-L urine in PANC-1 cells. (g&h) Reduction in Lrp5, Snail, MMP9, Runx2 by post-L urine in PC-3 and PANC-1 cancer cells.

Suppl. Figure S2.
Simvastatin's inhibitory and mevalonate's stimulatory effects on EO771 and MDA-MB-231 cells. The single and double asterisks indicate $p < 0.05$ and $p < 0.01$, respectively. Of note, CN = control, Sim = simvastatin, Me = mevalonate, pre-L = unconditioned UM, and post-L = loading-conditioned UM. (a) Effects of simvastatin on invasion capability in EO771 cells. (b) Expression of Lrp5, Snail, MMP9, PPARγ, and Runx2 in response to simvastatin in EO771 cells. (c) Effects of simvastatin on invasion capability in MDA-MB-231 cells. (d) Expression of Lrp5, Snail, MMP9, PPARγ, and Runx2 in response to simvastatin in MDA-MB-231 cells. (e) Effects of mevalonate on invasion capability in EO771 cells. (f) Expression of Lrp5, Snail, MMP9, PPARγ, and Runx2 in response to mevalonate in EO771 cells. (g) Effects of mevalonate on invasion capability in MDA-MB-231 cells. (h) Expression of Lrp5, Snail, MMP9, PPARγ, and Runx2 in response to mevalonate in MDA-MB-231 cells.

Suppl. Figure S3.
Effects of 2-Heptanone and 2-Pentanone on hypothalamic neuronal cells (GnRH), MDA-MB-231 cells, and EO771 cells. (A) Regulation of AANAT and TH in GnRH hypothalamic neuronal cells. (b&c) Effects on MTT-based cellular viability and expression of Lrp5, Snail, MMP9, and PPARγ in MDA-MB-231cells. (d&e) Effects on MTT-based cellular viability and expression of Lrp5, Snail, MMP9, and PPARγ in EO7711cells.

Suppl. Figure S4.
Effects of CSF1 on EO771 cells. (a) Promotion of cellular migration by CSF1 administration. (b) Elevation of Lrp5, Snail, MMP9 and PPARγ by CSF1 administration.

Suppl. Figure S5.
Effects of urine on PC-3 prostate cancer cells and PANC-1 pancreatic cancer cells. (a&b) Inhibition of MTT-based cellular viability and migration of PC-3 prostate cancer cells by loading conditioned UM. (c&d) Inhibition of MTT-based cellular viability and migration of PANC-1 pancreatic cancer cells by loading-conditioned UM. (e&f) Inhibition of cellular invasion and downregulation of Lrp5, Snail, MMP9, PPARγ, and RUnx2 in PC-3 prostate cancer cells by loading-conditioned UM. (g&h) Inhibition of cellular invasion and downregulation of Lrp5,

Snail, MMP9, PPARγ, and RUnx2 in PANC-1 pancreatic cancer cells by loading-conditioned UM. (i) pH of human urine.

Supplementary Figures

Suppl. Figure S1.

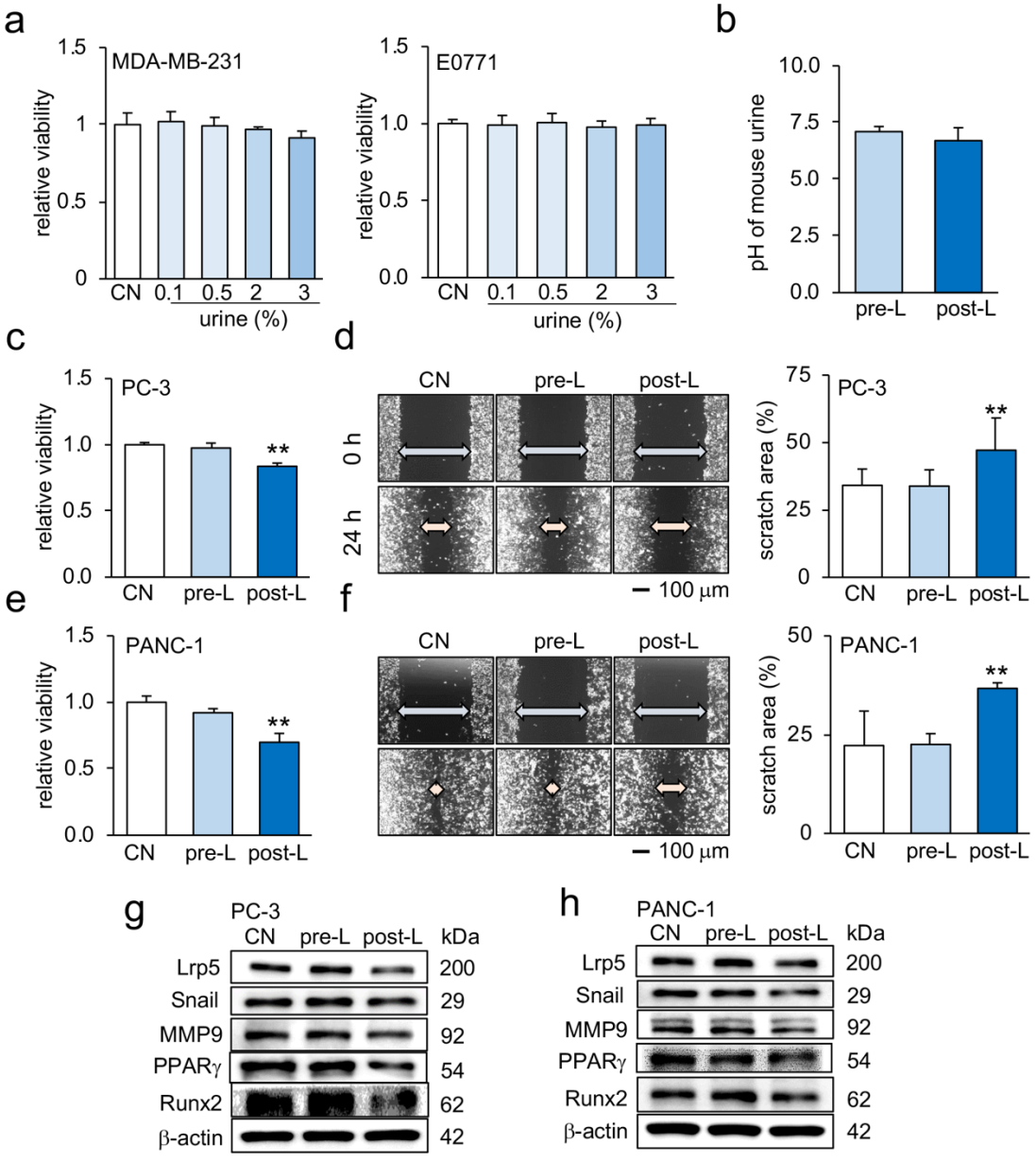

Suppl. Figure S2.

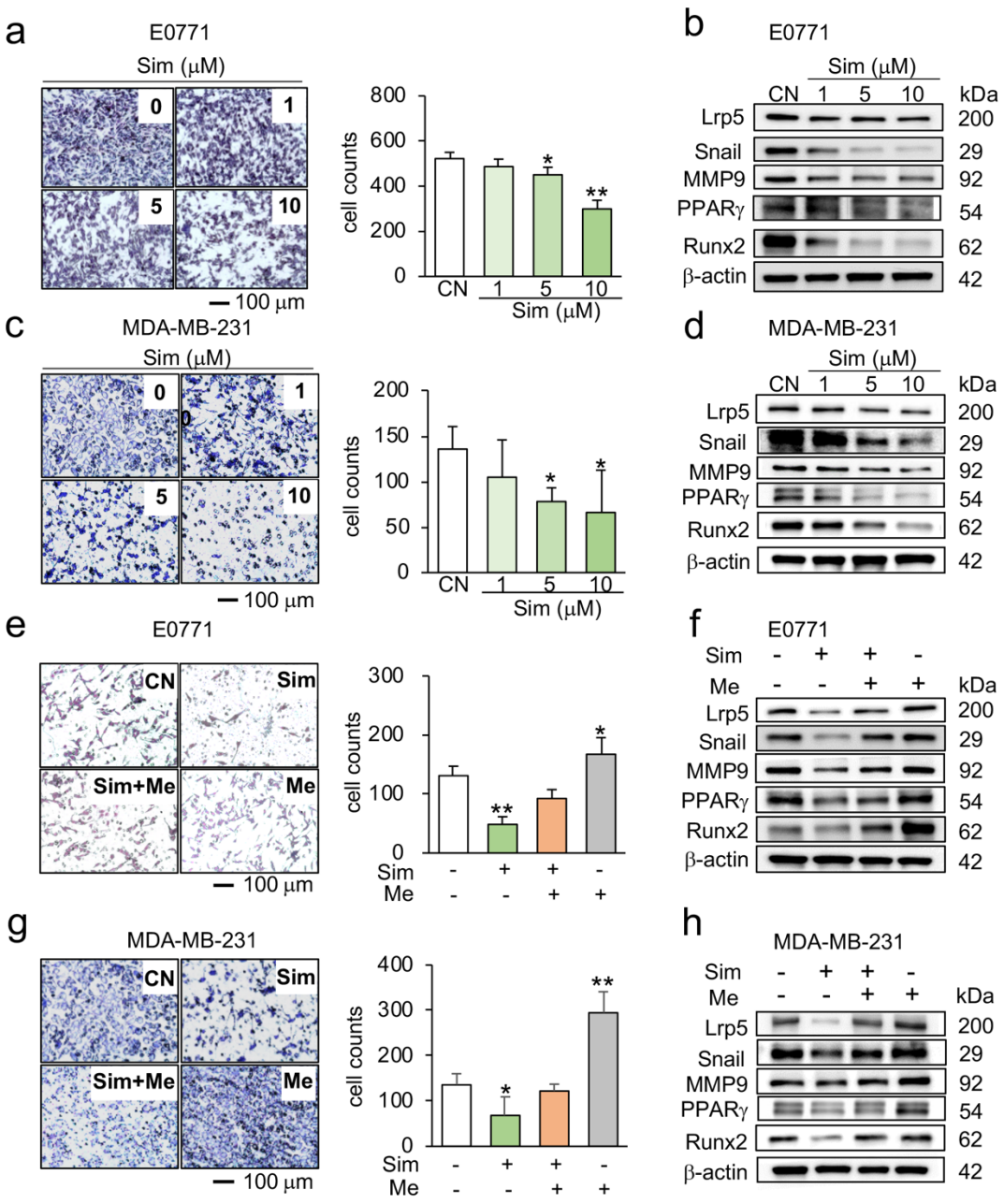

Suppl. Figure S3.

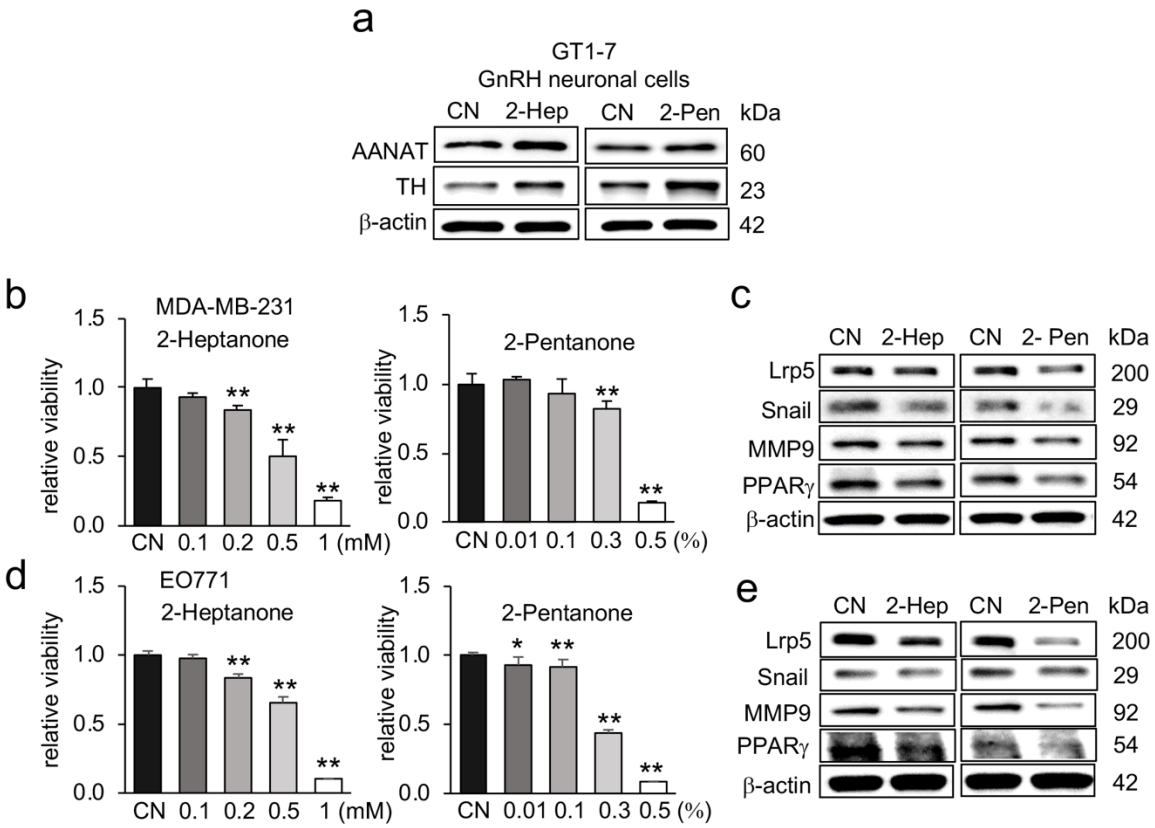

Suppl. Figure S4.

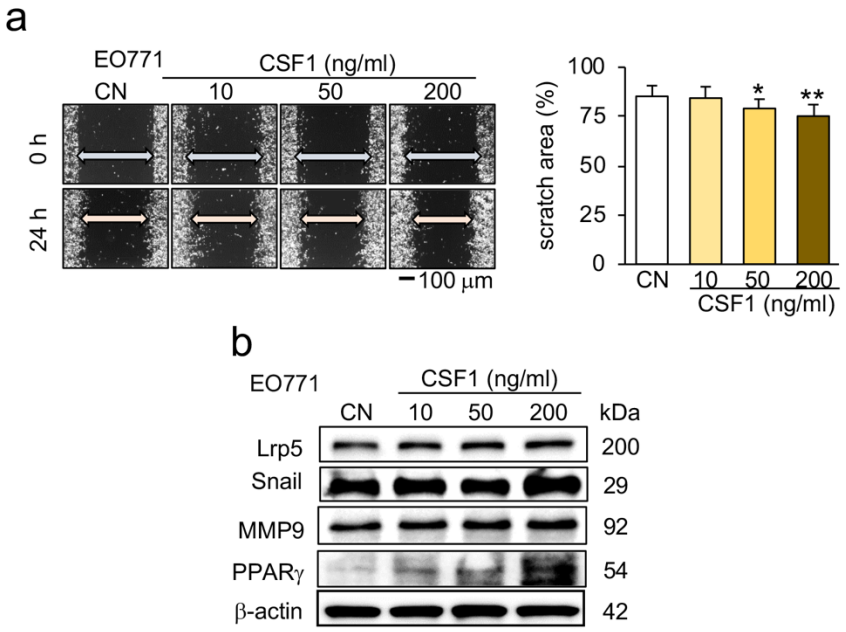

Suppl. Figure S5.